Journal of Alloys and Compounds 509 (2011) 571–577

Contents lists available at ScienceDirect

Journal of Alloys and Compounds

journal homepage: www.elsevier.com/locate/jallcom

Electronic properties of Al/DNA/p-Si MIS diode: Application as temperature sensor

Ö. Güllü [a,b,*], A. Türüt [c]

[a] Batman University, Science and Art Faculty, Department of Physics, 72060 Batman, Turkey
[b] Osmaniye Korkut Ata University, Science and Art Faculty, Department of Physics, 80000 Osmaniye, Turkey
[c] Atatürk University, Science Faculty, Department of Physics, 25240 Erzurum, Turkey

ARTICLE INFO

Article history:
Received 13 April 2010
Received in revised form
22 September 2010
Accepted 26 September 2010
Available online 20 October 2010

Keywords:
Silicon
DNA
Metal–semiconductor structures
Barrier height
Ideality factor

ABSTRACT

The current–voltage (I–V) measurements were performed in the temperature range (200–300 K) on Al/DNA/p-Si Schottky barrier type diodes. The Schottky diode shows non-ideal I–V behaviour with ideality factors n equal to 1.34 ± 0.02 and 1.70 ± 0.02 at 300 K and 200 K, respectively, and is thought to have a metal-interface layer-semiconductor (MIS) configuration. The zero-bias barrier height Φ_b determined from the I–V measurements was 0.75 ± 0.01 eV at 300 K and decreases to 0.61 ± 0.01 eV at 200 K. The forward voltage–temperature (V_F–T) characteristics were obtained from the I–V measurements in the temperature range 200–300 K at different activation currents (I_F) in the range 20 nA–6 μA. The V_F–T characteristics were linear for three activation currents in the diode. From the V_F–T characteristics at 20 nA, 100 nA and 6 μA, the values of the temperature coefficients of the forward bias voltage (dV_F/dT) for the diode were determined as $-2.30\,mV\,K^{-1}$, $-2.60\,mV\,K^{-1}$ and $-3.26\,mV\,K^{-1}$ with a standard error of $0.05\,mV\,K^{-1}$, respectively.

1. Introduction

Semiconducting organic materials are of particular interest, since they possess advantageous electrical, optoelectronic and processing properties for design and fabrication of novel class of the semiconductor-based devices such as diodes, photovoltaic devices [1,2]. Attractive features of these materials are possibility of device processing, compatibility with flexible substrates, and the low materials consumption for ultra thin molecular films, all of which offer the prospect of cheaper photovoltaic energy generation [3,4]. The electrical properties of metal/semiconductor (MS) structures can be modified by organic semiconductors when an organic layer is inserted between the inorganic semiconductor and metal. The studies made in literature have shown that the barrier height could be either increased or decreased by using organic thin layer on inorganic semiconductor [1–11]. New electrical properties of the MS contacts can be promoted by means of the choice of suitable organic semiconductors [1]. Among those, DNA is considered to be a good candidate for organic semiconductor devices fabrication such as metal-interfacial layer-semiconductor (MIS) diodes and solar cells [12]. Deoxyribo nucleic acid (DNA), the blueprint of life, has taken centre stage in bio-physical chemistry research during the past few decades [13]. In molecular-scale systems, DNA, is one of the most promising materials because they have several unique advantages [14]; such as nanometer-scale molecular film, adjustable length, and self-assembly property [15–17]. Recent studies [18–22] on the electrical conduction of the DNA molecules reveal that they may act as either semiconductor with nano-size dimensions or non-semiconductor materials (i.e., insulator or metal) [23]. The latest review [24] appears to favor the viewpoint that DNA is an insulator, or at least a wide band gap semiconductor with nonlinear I–V (current–voltage) characteristics [25]. This view point is supported by the measurements of Porath et al. [18] and Rakitin et al. [26].

The reliability and usefulness of semiconductor electronic devices in integrated circuit or other applications is based on the stability of the characteristic parameters of diodes over a wide range of temperature. The analyses of the current–voltage (I–V) characteristics of the Schottky diodes obtained only at room temperature showed that it does not give detailed information about the charge transport process and about the nature of the barrier formed at the metal–semiconductor interface. The temperature dependence of the I–V characteristics gives a better picture of the conduction mechanism and allows one to understand different aspects that shed light on the validity of various processes involved [27–29]. Although the thermionic emission theory is used to extract the Schottky barrier diode (SBD) parameters, in many cases the

* Corresponding author at: Batman University, Science and Art Faculty, Department of Physics, 72060 Batman, Turkey. Tel.: +90 488 217 3620; fax: +90 488 215 7201.
E-mail address: omergullu@gmail.com (Ö. Güllü).

0925-8388/$ – see front matter © 2010 Elsevier B.V. All rights reserved.
doi:10.1016/j.jallcom.2010.09.146

barrier height and the ideality factor determined from forward *I–V* characteristics are found to be a function of temperature. The evaluation of the experimental current–voltage data show in these cases that there is a decrease in the zero-bias barrier height (BH) and an increase in the ideality factor with decreasing temperature [28–33]. The decrease in the barrier height at low temperatures may lead to non-linearity in the activation energy $\ln(I_0/T^2)$ versus $1/T$ plot. Some authors [27–33] have used an approximation on the basis of a thermionic emission mechanism with Gaussian distribution of barrier heights around a mean value to explain the nature and origin of the decrease of barrier height and increase of ideality factor with a decrease in temperature and the non-linearity of the activation energy plot over a wide temperature range.

In this work, we report the study of the current transport characteristics of Al/DNA/p-Si Schottky diodes in the temperature range (200–300 K). The forward *I–V* characteristics were used to establish the current transport mechanism in Al/DNA/p-Si diodes as well as to estimate the variation of the ideality factor n and the barrier height Φ_b at different temperatures. The same measurements were also exploited to determine the characteristic energy E_{00}.

2. Experimental details

2.1. Chemical cleaning and ohmic contact formation

MIS diodes were prepared by using one side polished (as received from the manufacturer) *p*-type Si wafers (boron doped) with (1 0 0) orientation and 1.19×10^{15} cm^{-3} doping density from capacitance–voltage (*C–V*) measurements. Si wafers were purchased from University Wafer (South Boston, MA). The wafer was chemically cleaned by using the RCA cleaning procedure (i.e. a 10 min boil in $NH_3 + H_2O_2 + 6H_2O$ followed by a 10 min boil in $HCl + H_2O_2 + 6H_2O$). The native oxide on the front surface of the substrates was removed in HF:H_2O (1:10) solution and finally was rinsed in de-ionized water for 30 s. All reagents and solvents were purchased in their highest available purity and used without further purification. Deionized water (18 MΩ) was used in all experiments. Low resistivity ohmic back contact to *p*-type Si substrate was formed by using Al metal with the purity of 99.99%, followed by a temperature treatment at 570 °C for 3 min in N_2 atmosphere.

2.2. Deposition of DNA and top contact metallization

Genomic DNA isolation was described in Miller et al. [34]. The purity of DNA was 1.80 (A260/A280 absorbance ratio). After the cleaning and ohmic metallization procedures, DNA thin film has directly been formed by a simple cast method by adding 10 μL DNA solution with a concentration of 200 μg/ml in water on the front surface of the p-Si wafer and has been evaporated by itself for drying of solvent in N_2 atmosphere for one day. Here, we have selected an amount of 10 μL of DNA solution by considering and testing various factors that could effect a given organic film thickness and homogeneity depending on the solution concentration and substrate area. The quality of organic thin films should be also related to other factors, such as the film-forming ability, the molecular symmetry and structure [35]. Additionally, it is well known that interactions between DNA molecules and surfaces involve electrostatic forces as well as long-range van der Waals forces and dipole–dipole interactions, so the selection of substrates used for DNA devices is very important for the adhesion of DNA on substrates during experiment [36]. We have observed that the adhesion between DNA and silicon was not enough good in our experiments. But, Gao and Park [36] have recently showed that chemical surface treatments such as plasma etching on silicon substrate increased adhesion between DNA and silicon. They [36] have reported that the improved adhesion with plasma treatments could be understood on the basis of the generation of parasitic charges in the treated surface which interacted electrostatically with the DNA molecules. Also, we have not measured surface smoothness of DNA layer on Si, because we have no imaging system. But, some studies have recently been performed about smoothness of DNA on the substrates. For example, Okur et al. [37] have reported that the topography showed a smooth and completely covered DNA film surface, while the film disorders and pinholes of DNA on the silicon substrate could be clearly distinguished from the contrast of the AFM phase image. Also, Zhang et al. [38] have reported that the average roughness for DNA layer on a silicon substrate was calculated to be 5.1 nm, indicating that the film was relatively smooth. Thickness of the DNA film on the Si substrate has been calculated as (61 ± 5) nm from high frequency *C–V* technique. The contacting top metal dots with diameter of 1.0 mm have been formed by evaporation of Al. All metal evaporation processes have been carried out in a Leybold Heraeus Turbo Molecular High Vacuum Pump at about 10^{-5} Torr.

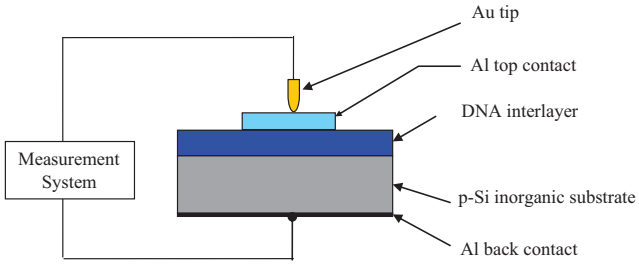

Fig. 1. The components of the Al/DNA/p-Si Schottky device for the electrical characterization. *Note*: Gold tip was used for saving the Al/DNA/p-Si structure from contact damages as DNA is very soft material.

2.3. Electrical measurements

The electrical measurements of the device (see Fig. 1) were taken in the temperature range of 200–300 K by using a Leybold Heraeus closed-cycle helium cryostat that enables us to make measurements in the temperature range of 10–340 K, and a Keithley 487 Picoammeter/Voltage source in dark conditions. Electrical measurements on Al top side of the diode are taken with gold tips for saving the Al/DNA/p-Si structure from contact damages as DNA is very soft material as seen in Fig. 1. The sample temperature was always monitored by a copper-constantan thermocouple and a Windaus MD850 electronic thermometer with sensitivity better than ±0.1 K.

3. Results and discussion

When MIS diodes with a thin interfacial layer are considered, it is assumed that the forward bias current of the device for $qV \gg 3kT$ is due to thermionic emission current and it can be expressed as [39]:

$$I = I_0 \quad \exp\left(\frac{qV}{nkT}\right) \tag{1}$$

where

$$I_0 = AA^*\theta T^2 \exp\left(\frac{-q\Phi_{b,0}}{kT}\right) \tag{2}$$

is the saturation current, k is Boltzmann constant, T is the temperature, $\Phi_{b,0}$ is the barrier height without interfacial layer, A^* is the effective Richardson constant and equals 32 A/cm^{2}K^2 for *p*-type Si, A is the diode area, θ is the transmission coefficient across the interfacial layer (DNA film) and is given in [39]. n is an ideality factor and is a measure of conformity of the diode to pure thermionic emission and it is determined from the slope of the straight line region of the forward bias $\ln(I–V)$ characteristics through the relation:

$$n = \frac{q}{kT}\frac{dV}{d(\ln I)} \tag{3}$$

In the usual analysis of the experimental data on Schottky contacts, the barrier height is determined from the extrapolated I_0. However, this is an apparent barrier height Φ_b when an interfacial layer is present. The effective or measured barrier height Φ_b is given by

$$\Phi_b = \frac{kT}{q}\ln\left(\frac{A^*AT^2}{I_0}\right) \tag{4}$$

By using Ref. [36], the measured barrier height can be written as:

$$\Phi_b = \Phi_{b,0} + \Phi_{b,\theta} \tag{5}$$

where $\Phi_{b,\theta}$ is the additional barrier due to effect of the interlayer (DNA film) for such as structures and is given in [39].

I–V measurement is one of the mostly used methods to determine the transport mechanism in diodes. In order to get further insights into the mechanism of current transport through the Al/DNA/p-Si contact, the *I–V* characteristics were performed at different temperatures in the range of 200–300 K. Fig. 2 shows the

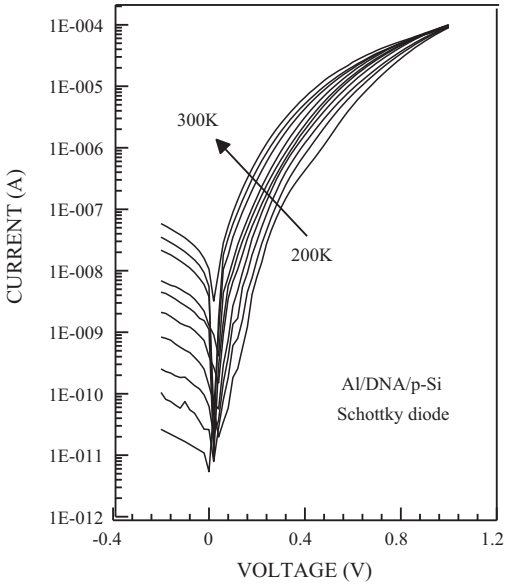

Fig. 2. Current–voltage characteristics of the Al/DNA/p-Si device as a function of temperature between 200 and 300 K.

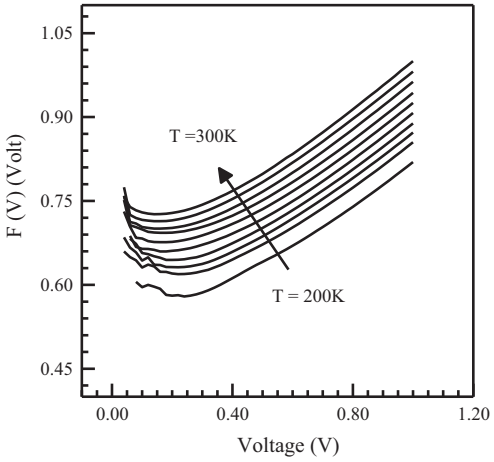

Fig. 4. F(*V*) *vs. V* characteristics of the Al/DNA/p-Si device as a function of temperature between 200 and 300 K.

Table 1
Some electrical parameters obtained by using Norde fuctions from temperature dependent *I–V* characteristics of Al/DNA/p-Si diode.

T (K)	Φ_b (eV)	R_S (kΩ)
300	0.770	78
290	0.760	111
280	0.746	165
270	0.750	206
260	0.734	259
250	0.718	253
240	0.714	281
230	0.722	278
220	0.702	316
200	0.680	286

semi-logarithmic plot of the *I–V* curves of the Al/DNA/p-Si diode at various temperatures. In order to find out ohmicity of Al top contact metal, it has also been investigated the linear *I–V* characteristic of Al/DNA/Al contact shown in the Fig. 3. This figure shows that there is a good ohmic behavior between the Al and the DNA layer. Fig. 2 depicts that a change in the *I–V* characteristics occurs by depending on sample temperature. As clearly seen from Fig. 2, the Al/DNA/p-Si Schottky structure exhibits excellent rectifying behavior. The weak voltage dependence of the reverse-bias current and the exponential increase of the forward-bias current are characteristic properties of rectifying interfaces. The current curve in forward bias quickly becomes dominated by series resistance from contact wires or bulk resistance of the organic material and inorganic semiconductor, giving rise to the curvature at high current in the semi-log *I–V* plot. Temperature dependent Norde curves were shown in Fig. 4. By using Norde method (please see Ref. [40] for more information), the series resistance R_s and barrier height (BH) values as a function of temperature were given in Table 1. The values of the series resistance and the barrier height from each Norde plots at different temperatures were shown in Fig. 5. As seen from this figure, the barrier height decreases with decreasing temperature and then the series resistance increases slightly.

The experimental values of ideality factor and barrier height obtained from the linear regions of the ln(*I–V*) characteristics by using the thermionic emission (TE) theory [39] for Al/DNA/p-Si diode are presented in Fig. 6. And, both values as a function of temperature are given in Table 2. Both parameters exhibit a temperature dependency as seen in Fig. 6. The experimental values of barrier heights Φ_b and ideality factors *n* ranged from 0.61 ± 0.01 eV and 1.70 ± 0.02 at 200 K to 0.75 ± 0.01 eV and 1.34 ± 0.02 at 300 K

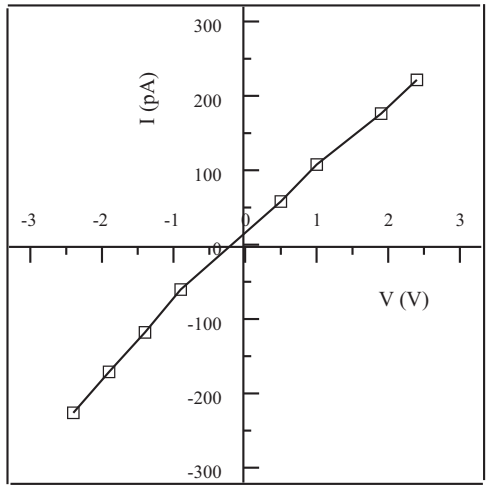

Fig. 3. Current–voltage characteristic of the Al/DNA/Al structure at room temperature.

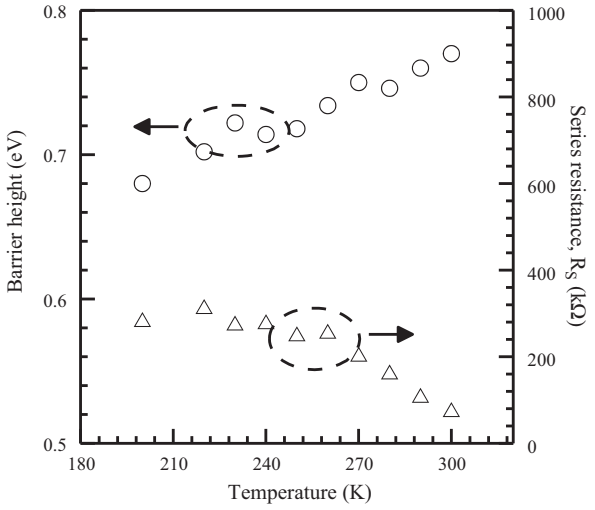

Fig. 5. Temperature dependence of the series resistance and the barrier height obtained from Norde method.

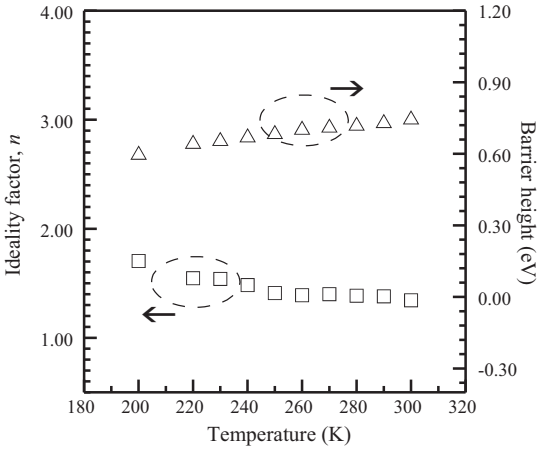

Fig. 6. Temperature dependences of experimental Φ_b and n values obtained from current *vs.* voltage characteristics of Al/DNA/p-Si device between 200 and 300 K.

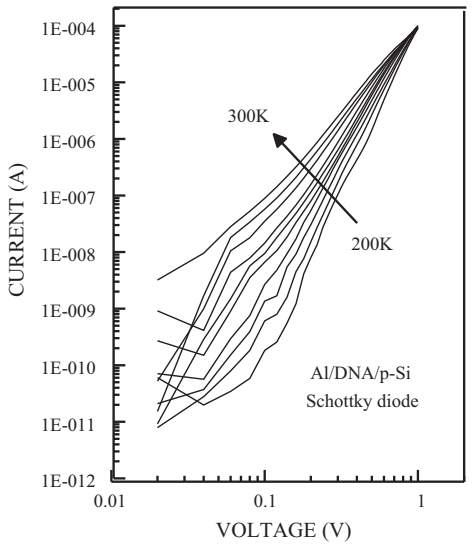

Fig. 7. Log(I)–log(V) characteristics of the Al/DNA/p-Si device as a function of temperature between 200 and 300 K.

for Al/DNA/p-Si diode, respectively. The ideality factor determined by the image-force effect alone should be close to 1.01 or 1.02 [41–44]. At room temperature, our data clearly indicate that the diode has the ideality factor that is significantly larger than this value. Higher values of ideality factors are attributed to secondary mechanisms which include interface dipoles due to interface doping or specific interface structure as well as fabrication-induced defects at the interface [41–44]. According to Tung [44], the high values of n can also be attributed to the presence of a wide distribution of low-BH patches caused by laterally barrier inhomogeneous. Also, the image-force effect, recombination-generation, and tunneling may be possible mechanisms that could lead to an ideality factor value greater than unity [44,45].

As seen from Fig. 6, while the barrier height Φ_b decreases, the ideality factor n increases with decreasing temperature. Because of the temperature activated process, the current transport will be dominated by current flowing through of the lower BH and a larger ideality factor [46]. That is, more electrons have sufficient energy to overcome the higher barrier when temperature increases and then, BH increases with temperature and bias voltage. Furthermore, an apparent increase in ideality factor and decrease in BH at low temperatures are possibly caused by some other effects (inhomogeneities of interface layer thickness and non-uniformity of the interfacial charges, etc.) giving rise to an extra current such that the overall characteristics still remain consistent with the TE process [47].

Generally, the experimental current–voltage characteristics can be treated by using an empirical relation of the form $I\ (V,T)\alpha \exp(eV/nkT)$. A careful examination of the I–V–T curves of the present diode revealed that the behavior of their forward current at intermediate and high bias voltages cannot be reliably analyzed using such an empirical formula even when it is modified by the incorporation of a series resistance effect over a limited narrow bias region. These results imply that additional transport mechanisms are dominant in these devices. This suggests that conduction processes occurring in the highly resistive DNA layer of the Al/DNA/p-Si diode would be a possible alternative candidate in determining its forward current in the intermediate and high bias regimes beyond that of the low bias diode-like behavior. To understand more clearly the electrical properties of the Al/DNA/p-Si diode, its I–V characteristics were plotted on log–log scale. Fig. 7 illustrates the forward bias log I versus log V plots of the Al/DNA/p-Si diode at different temperatures. As can be seen from Fig. 7, the double-logarithmic forward bias I–V plots show a good linearity in the range of 0.2–1.0 V, along with the best-fit power-law curve. The values of the power-law parameter, m, were calculated from the slopes of the linear portions of the double-logarithmic I–V plots under forward bias of the Al/DNA/p-Si heterojunction for each measurement temperature in the temperature range between 200 K and 300 K as given in Table 3. Fig. 8 shows a plot of m *vs.* 1000/T, which is fitted by a straight line corresponding to $T_c = 1648.5 \pm 0.5$ K, which T_c is the characteristic temperature parameter of the trap distribution. As can be seen from Fig. 8, the exponent m seems to increase with decreasing temperature, as expected for space charge limited current (SCLC) conduction [48–53]. This behavior can be used to derive the characteristic trap energy E_t from the temperature dependence of $E_t = kT_c$. The m *vs.* 1000/T plot shows a linear dependence slope yielding a trap energy of about 0.14 ± 0.01 eV from $E_t = kT_c$, and it can be said that most of the traps are deep traps as required by a E_t value of 0.14 ± 0.01 eV. In this study, the charac-

Table 2
Basic diode parameters extracted from I–V measurements as a fuction of temperature.

T (K)	n	Φ_b (eV)	I_0 (A)
300	1.344	0.753	5.10×10^{-9}
290	1.380	0.738	3.27×10^{-9}
280	1.386	0.727	1.69×10^{-9}
270	1.400	0.719	7.18×10^{-10}
260	1.390	0.710	3.01×10^{-10}
250	1.410	0.692	1.81×10^{-10}
240	1.483	0.678	8.44×10^{-11}
230	1.540	0.663	4.13×10^{-11}
220	1.546	0.651	1.52×10^{-11}
200	1.704	0.605	6.06×10^{-12}

Table 3
Power-law parameter, m values extracted from log I–log V characteristics of Al/DNA/p-Si diode as a function of temperature.

T (K)	1000/T (K^{-1})	m
300	3.08	3.33
290	3.32	3.45
280	3.58	3.57
270	4.06	3.70
260	4.31	3.85
250	4.52	4.00
240	4.69	4.17
230	4.95	4.35
220	5.38	4.55
200	5.79	5.00

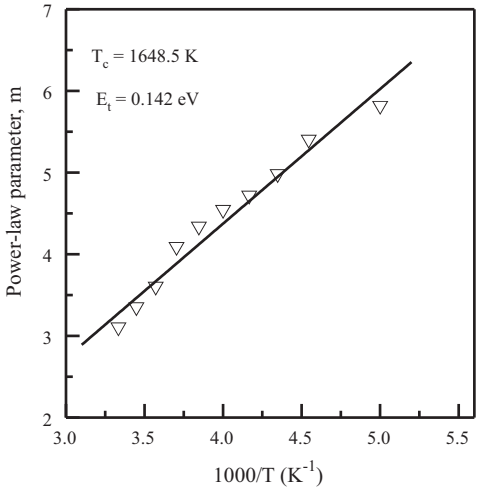

Fig. 8. The m versus 1000/T characteristic of the Al/DNA/p-Si device as a function of temperature between 200 and 300 K.

teristic energy obtained for DNA film is 0.14 ± 0.01 eV, comparable with the reported for polyaniline emeraldine base films (0.11 eV) prepared by the solution-casting technique [53]. At voltage region of 0.2–1.0 V, the forward I–V characteristics in the temperature range 200–300 K are influenced by the transport properties of the highly resistive DNA layer [48–53]. That is, the shape of the I–V characteristics is not only controlled by the contacts, but strongly depends on the nature of the DNA layer between the Al electrode and the p-Si semiconductor. Generally, double-logarithmic forward bias I–V plots with a slope equal to or larger than 2 suggest the possibility of the SCLC mechanism [50–54]. The double-logarithmic forward bias I–V curves in Fig. 7 show a power-law behavior of the current, $I \propto V^{(m+1)}$, with different exponents $(m+1)$. That is, such power laws with exponents larger than two have been interpreted as an indication of trap-charge-limited conduction with an exponent trap distribution [50,51]. The SCLC conduction should become important when the density of injected free-charge carriers is much larger than the thermally generated free-charge carrier density. In this study, the injected charge carriers can proceed through the junction from the moderately doped p-Si ($N_a = 1.19 \times 10^{15}$ cm^{-3}) into the highly resistive DNA material with much lower concentration of free holes to sustain a flow of trap-charge-limited current. Thus, it is possible to recognize the effect of traps on the conduction current which is dominated by an exponential distribution of traps at corresponding voltage region. Traps are locations arising from disorders, dangling bonds, impurities, etc., and are called localized states that very often capture free-charge carriers, playing a very important role in the conduction process of an organic layer [56]. Similarly transport phenomena have been observed in dielectrics, amorphous semiconductors, wide band gap semiconductors, and other organic solids [48–56].

It is observed that n is greater than 1 and this is an indication that thermionic emission is not the only operative mechanism for current flow and is usually attributed to a Schottky barrier height which is bias dependent. If the current transport is controlled by the thermionic field emission (TFE) theory, the relation between current and voltage can be expressed as [57,58].

$$I = I_0 \exp\left(\frac{V}{E_0}\right) \tag{6}$$

with

$$E_0 = E_{00} \coth\left(\frac{qE_{00}}{kT}\right) = \frac{nkT}{q} \tag{7}$$

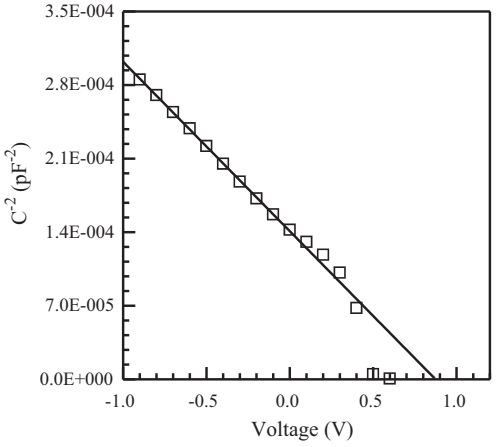

Fig. 9. Capacitance^{-2}–voltage (C^{-2}–V) characteristic of the diode from C–V measurement at room temperature at 500 kHz.

where E_{00} is the characteristic energy, which is related to the transmission probability of the carrier through the barrier given in the following equation:

$$E_{00} = \frac{h}{4\pi}\sqrt{\frac{N_a}{m_e^* \varepsilon_s}} \tag{8}$$

where h is the Planck constant, N_a is the acceptor concentration, ε_s is the semiconductor dielectric constant and m_e^* is the electron effective mass.

In the case of our Al/DNA/p-Si Schottky diode, with $N_a = 1.19 \times 10^{15}$ cm^{-3}, determined from the capacitance-voltage measurement as seen from C^{-2}–V plot in Fig. 9, $m_e^* = 0.16 m_0$ [59] and ($\varepsilon_s = 11.9\varepsilon_0$) the value of E_{00} turns out to be 0.40 meV.

Using the experimental values, the increase in ideality factor is further analysed by considering the tunneling current as the cause for the variation of the ideality factor n. Fig. 10 shows a plot of E_0 versus kT/q. The value of E_0 is determined from Eq. (7). A linear fit to the data results in a y-intercept, which gives a value of E_0 as 7.07 ± 0.05 meV. This fit is good down to a temperature of 250 K and deviates below this temperature. The experimentally observed E_0 value of 7.07 ± 0.05 meV at ($T = 0$ K) obtained from $E_{00} = f(kT/q)$ data (Fig. 10) was higher about 18 times than the theoretically calculated value of $E_{00} = 0.40$ meV. In our study, as seen in Fig. 10, E_0 *vs.* kT/q plot shows a dependence that is usually attributed to a domination of the conduction mechanism by TFE. However, temperature

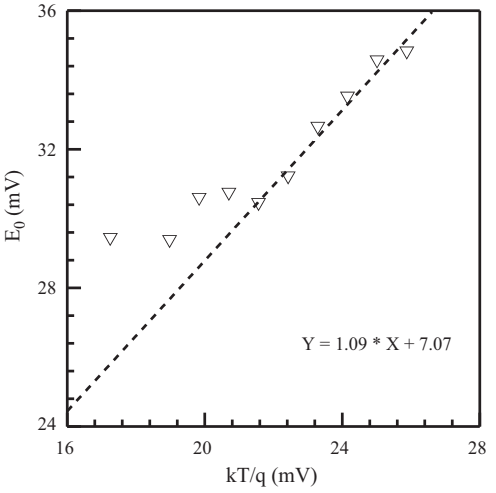

Fig. 10. Variation of E_0 versus kT/q for Al/DNA/p-Si device.

dependence similar to the curve including experimental values have often been observed under experimental conditions where tunneling should be negligible [44]. The evaluated ideality factors are shown in Fig. 10, which qualitatively reproduces the behavior usually attributed to the TFE mechanism. Thus, even though tunneling should dominate the electron conduction at heavily doped MIS junctions, TFE is not necessarily for the conduction mechanism whenever dependence like that in Fig. 10 is observed. The temperature dependence of the ideality factor, by itself, does not provide a determination of conduction mechanism [44].

The experimentally observed values of $1/n$ (open triangels) were superimposed on theoretically generated $1/n$ versus $1000/T$ plots in Fig. 11. This plot provides a good check to know whether the conduction mechanism is TFE or TE. The temperature dependence of the experimental ideality factor is in agreement with the solid curve obtained with $E_{00} = 27$ meV for Al/DNA/p-Si diode in the temperature range 200–300 K. Thus, it can be seen that there is a significant consistency between the theoretical and experimental characteristics in related temperature range. This value of the characteristic energy value E_{00} is higher about 70 times than the theoretical value of 0.40 meV. To understand the possible origin of the high characteristic energy, it should be underlined that E_{00} is connected with the transmission probability [59–62]. On one hand, it characterizes the electric field at the semiconductor surface for an applied bias through the carrier concentration and dielectric constant. So, it determines the barrier shape and width. On the other hand, it characterizes the density of states through the effective mass. Therefore, any mechanism which enhances the electric field or the density of states at the semiconductor surface will increase the thermionic-field emission, and so the apparent E_{00} [63,64].

For the evaluation of the BH, one may also use Richardson plots from saturation currents. Fig. 12 shows a conventional activation energy $\ln(I_0/T^2)$ *vs.* $1/kT$ plot (indicated by open triangels) according to TE theory [39] for Al/DNA/p-Si diode. Experimental $\ln(I_0/T^2)$ versus $1/kT$ plot shows a significant deviation from linearity at low temperatures, whereas the plot of $\ln(I_0/T^2)$ *vs.* $1/nkT$ (open circles) is linear in the temperature range 200–300 K with a slope giving an activation energy of 0.99 ± 0.01 eV within the experimental error. The experimental data for $1/kT$ plot are seen to be fitted asymptotically to a straight line at higher temperatures only. The activation energy value from the slope of this straight line have been obtained as 0.41 ± 0.01 eV for $1/kT$ (Fig. 12). Bowing of the experimental $\ln(I_0/T^2)$ *vs.* $1/kT$ curve may be caused by the temperature dependence of the BH and ideality factor n due to the existence of the surface inhomogeneities of the Si substrate [60–62,65–67]. Also, the deviation in the Richardson plots may be due to the spatially inhomogeneous BHs and potential fluctuations at the interface that consist of low and high barrier areas [60–63,65–67]. That is, the current through the diode will flow preferentially through the lower barriers in the potential distribution.

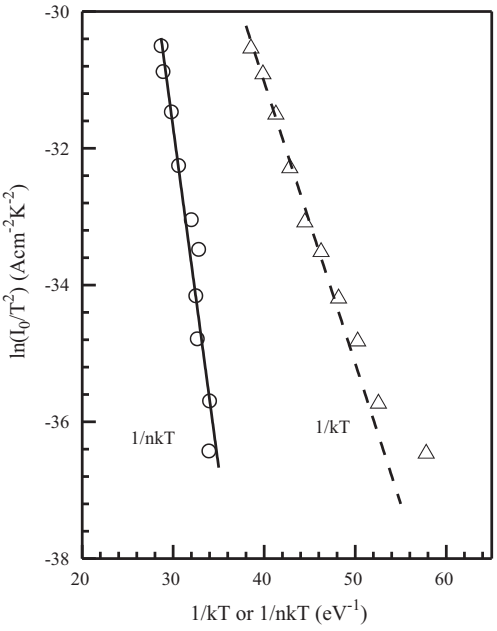

Fig. 12. $\ln(I_0/T^2)$ *vs.* $1/nkT$ (indicated by open circles) and $1/kT$ (open triangles) Richardson plots obtained from experimental *I–V* characteristics for Al/DNA/p-Si.

The forward voltage–temperature (V_F–T) characteristics for the Al/DNA/p-Si diode were obtained from the *I–V* measurements in the temperature range 200–300 K at different activation currents (I_F) in the range $20\ \text{nA} < I_F < 6\ \mu\text{A}$. The V_F–T plots at different I_F levels for the diode are shown in Fig. 13. V_F values as a function of temperature at different activation currents (I_F) in the range $20\ \text{nA} < I_F < 6\ \mu\text{A}$ were given in Table 4. The forward voltage (V_F) exhibited a linear dependence on temperature for three activation currents in the diode (Fig. 13). From the V_F–T characteristics at 20 nA, 100 nA and 6 μA, the values of the temperature coefficients of the forward bias voltage (dV_F/dT) for the diode were determined

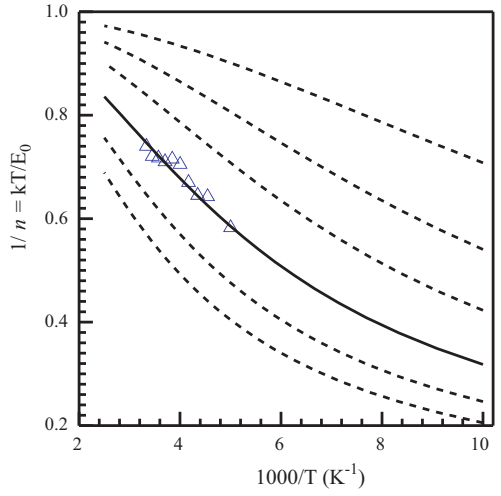

Fig. 11. Variation of $1/n$ versus $1000/T$ with E_{00} as the parameter for Al/DNA/p-Si device. The open triangels show the temperature dependence values of experimental ideality factor obtained from the current–voltage characteristics.

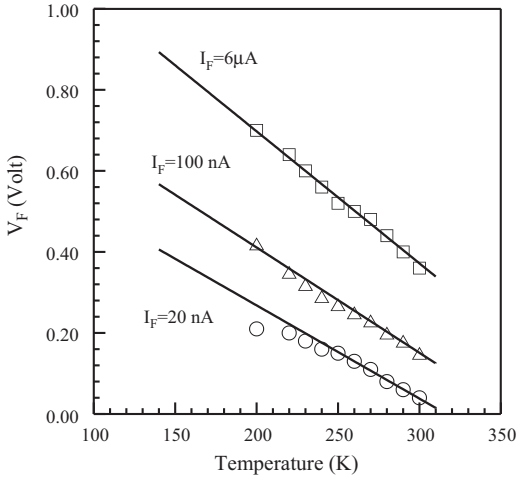

Fig. 13. V_F–T characteristics of the Al/DNA/p-Si Schottky diode activated at different currents.

Table 4
V_F values obtained from I–V characteristics for different I_F values as a function of temperature.

T (K)	V_F (V)		
	I_F = 20 nA	I_F = 100 nA	I_F = 6 μA
300	0.04	0.15	0.36
290	0.06	0.18	0.40
280	0.08	0.20	0.44
270	0.11	0.23	0.48
260	0.13	0.25	0.50
250	0.15	0.27	0.52
240	0.16	0.29	0.56
230	0.18	0.32	0.60
220	0.20	0.35	0.64
200	0.21	0.42	0.70

as $-2.30\,mV\,K^{-1}$, $-2.60\,mV\,K^{-1}$ and $-3.26\,mV\,K^{-1}$ with a standart error of $0.06\,mV\,K^{-1}$, respectively. The values of the slope (dV_F/dT) increased in the diode with the increase in the activation current, I_F. These values of the slope (dV_F/dT) for Al/DNA/p-Si diode agree with the values obtained by the reference [68]. Moreover, the value of slope $dV_F/dT = -3.26\,mV\,K^{-1}$ at I_F = 6 μA in the diode was higher than the value of $-2.30\,mV\,K^{-1}$ for the commercial Si p–n junction [69]. In other words, the fact that the sensibility of the Al/DNA/p-Si Schottky diode as temperature sensor is 42% higher than that of a Si p–n junction, indicates that the Al/DNA/p-Si Schottky diode is a good alternative as thermometer sensor.

4. Conclusion

This work reported here proposes that DNA molecules should be considered, among other candidates, as a potential organic thin film for metal-interface layer-semiconductor devices. In summary, we studied the I–V characteristics of Al/DNA/p-Si diodes in the temperature range (200–300 K). This device with MIS configuration shows non-ideal I–V behaviour. Ideality factors were 1.34 ± 0.02 and 1.70 ± 0.02 at 300 K and 200 K, respectively. Φ_b value determined from the I–V measurements was 0.75 ± 0.01 eV at 300 K and decreases to 0.61 ± 0.01 eV at 200 K. V_F–T characteristics were extracted from the I–V measurements as a function of temperature at different I_F values in the range 20 nA–6 μA. The V_F–T plots were linear for three activation currents in the device. From the V_F–T plots at 20 nA, 100 nA and 6 μA, the values of the temperature coefficients of the forward bias voltage (dV_F/dT) for the diode were determined as $-2.30\,mV\,K^{-1}$, $-2.60\,mV\,K^{-1}$ and $-3.26\,mV\,K^{-1}$ with a standart error of $0.05\,mV\,K^{-1}$, respectively. The facts: (i) that the technology of the fabrication of a Al/DNA/p-Si Schottky diode much simpler and economical than that for the Si p–n junction and (ii) the sensibility of the Al/DNA/p-Si Schottky diode as temperature sensor is 42% higher than that of a Si p–n junction, indicate that the Al/DNA/p-Si Schottky diode is a good alternative as temperature sensor.

References

[1] M.E. Aydin, F. Yakuphanoglu, T. Kılıçoğlu, Synth. Met. 157 (2007) 1080.
[2] R.K. Gupta, K. Ghosh, P.K. Kahol, Physica E 41 (2009) 1832.
[3] K.R. Rajesh, C.S. Menon, J. Non-Cryst. Solids 353 (2007) 398.
[4] R.K. Gupta, K. Ghosh, P.K. Kahol, J. Yoon, S. Guha, Appl. Surf. Sci. 254 (2008) 7069.
[5] T. Kilicoglu, M.E. Aydin, Y.S. Ocak, Physica B 388 (2007) 244.
[6] S.R. Forrest, M.L. Kaplan, P.H. Schmidt, W.L. Feldmann, E. Yanowski, Appl. Phys. Lett. 41 (1982) 90.
[7] R.K. Gupta, R.A. Singh, Mater. Chem. Phys. 86 (2004) 279.
[8] M.E. Aydin, T. Kilicoglu, K. Akkilic, H. Hosgoren, Physica B 381 (2006) 113.
[9] S.R. Forrest, M.L. Kaplan, P.H. Schmidt, J. Appl. Phys. 55 (1984) 1492.
[10] S. Antohe, N. Tomozeiu, S. Gogonea, Phys. Stat. Sol. A 125 (1991) 397.
[11] M.A. Ebeoglu, T. Kilicoglu, M.E. Aydin, Physica B 395 (2007) 93.
[12] O. Gullu, A. Turut, Sol. Energy Mater. Sol. Cells 92 (2008) 1205.
[13] V. Bhalla, R.P. Bajpai, L.M. Bharadwaj, EMBO Rep. 4 (5) (2003) 442.
[14] J.S. Hwang, S.H. Hong, H.K. Kim, Y.W. Kwon, J.I. Jin, S.W. Hwang, D. Ahn, Extended Abstracts of the 2004 International Conference on Solid State Devices and Materials, Tokyo, 2004, p. 332.
[15] J.S. Hwang, S.W. Hwang, D. Ahn, Superlattices Microstruct. 34 (2003) 433.
[16] O. Gullu, M. Cankaya, O. Baris, M. Biber, H. Ozdemir, M. Gulluce, A. Turut, Appl. Surf. Sci. 254 (2008) 5175.
[17] C.A. Mirkin, R.L. Letsinger, R.C. Mucic, J.J. Storhoff, Nature 382 (1996) 607.
[18] D. Porath, A. Bezryadin, S. de Vries, C. Dekker, Nature 403 (2000) 635.
[19] A.Y. Kasumov, M. Kociak, S. Gueron, B. Reulet, V.T. Volkov, D.V. Klinov, H. Bouchiat, Science 291 (2001) 280.
[20] A.J. Storm, J. Van Noort, S. de Vries, C. Dekker, Appl. Phys. Lett. 79 (2001) 3881.
[21] L. Cai, H. Tabata, T. Kawai, Appl. Phys. Lett. 77 (2000) 3105.
[22] H.W. Fink, C. Schonenberger, Nature 398 (1999) 407.
[23] Y.S. Jo, Y. Lee, Y. Roh, Mater. Sci. Eng. C 23 (2003) 841.
[24] R.G. Endres, D.L. Cox, R.R.P. Singh, Rev. Mod. Phys. 76 (2004) 195.
[25] H.L. Kwok, IEE Proc. Nanobiotechnol. 151 (2004) 193.
[26] A. Rakitin, P. Aich, C. Papadopoulos, Y. Kobzar, A.S. Wedeneev, J.S. Lee, J.M. Xu, Phys. Rev. Lett. 86 (2001) 3670.
[27] S. Chand, J. Kumar, Semicond. Sci. Technol. 10 (1995) 1680.
[28] S. Chand, J. Kumar, Appl. Phys. A 63 (1996) 171.
[29] Zs.J. Horvath, J. Appl. Phys. 64 (1988) 6780.
[30] Y.P. Song, R.L. Van Mairhaeghe, W.H. Laflere, F. Cardon, Solid State Electron. 29 (1986) 633.
[31] S. Hardikar, M.K. Hudait, P. Modak, S.B. Krupanidhi, N. Padha, Appl. Phys. A 68 (1999) 49.
[32] S. Bandyopadhyay, A. Bhattacharya, S.K. Sen, J. Appl. Phys. 85 (1999) 3671.
[33] S. Aniltürk, R. Turan, Solid State Electron. 44 (2000) 41.
[34] A. Miller, D.D. Dykes, H.F. Polesky, Nucleic Acids Res. 16 (1988) 1215.
[35] Y. Qiu, J. Qiao, Thin Solid Films 372 (2000) 265.
[36] J. Gao, M.B. Chan-Park, Surf. Coat. Technol. 194 (2005) 244.
[37] S. Okur, F. Yakuphanoglu, M. Ozsoz, P.K. Kadayifcilar, Microelectron. Eng. 86 (2009) 2305.
[38] Y. Zhang, S. Yang, C. Liu, X. Dai, W. Cao, J. Xu, Y. Li, New J. Chem. 26 (2002) 617.
[39] E.H. Rhoderick, R.H. Williams, Metal–Semiconductor Contacts, 2nd ed., Clarendon, Oxford, 1988.
[40] S. Karatas, S. Altindal, A. Turut, M. Cakar, Physica B 392 (2007) 43.
[41] M. Cakar, N. Yildirim, S. Karatas, C. Temirci, A. Turut, J. Appl. Phys. 100 (2006) 074505.
[42] S.R. Forrest, M.L. Kaplan, P.H. Schmidt, J. Appl. Phys. 60 (1986) 2406.
[43] C.H. Chen, I. Shih, J. Mater. Sci.: Mater. Electron. 17 (2006) 1047.
[44] R.T. Tung, Phys. Rev. B 45 (1992) 13509.
[45] A. Bolognesi, A. Di Carlo, P. Lugli, T. Kampen, D.R.T. Zahn, J. Phys.: Condens. Matter 15 (2003) S2719.
[46] R.F. Schmitsdorf, T.U. Kampen, W. Monch, J. Vac. Sci. Technol. B 15 (1997) 1221.
[47] S. Altindal, S. Karadeniz, N. Tugluoglu, A. Tataroglu, Solid State Electron. 47 (2003) 1847.
[48] M.M.A. Jafar, Semicond. Sci. Technol. 18 (2003) 7.
[49] S. Aydogan, M. Saglam, A. Turut, J. Phys.: Condens. Matter 18 (2006) 2665.
[50] M.A. Lambert, P. Park, Current Injection in Solids, Academic, New York, 1970, p. 47.
[51] A.A. Grinberg, S. Luryi, M.R. Pinto, N.L. Schryer, IEEE Trans. Electron. Devices 36 (1989) 1162.
[52] X.M. Shen, D.G. Zhao, Z.S. Liu, Z.F. Hu, H. Yang, J.W. Liang, Solid State Electron. 49 (2005) 847.
[53] K.P. Nazeer, S.A. Jacob, M. Thamilselvan, D. Mangalaraj, S.K. Narayandass, J. Yi, Polym. Int. 53 (2004) 898.
[54] M. Kaya, H. Cetin, B. Boyarbay, A. Gok, E. Ayyildiz, J. Phys.: Condens. Matter 19 (2007) 406205.
[55] M.M. El-Nahass, K.F. Abd-El-Rahman, A.A. Farag, A.A.A. Darwish, Org. Elect. 6 (2005) 129.
[56] M.A. Ahmed, Kh.S. Karimov, S.A. Moiz, IEEE Trans. Electron. Devices 51 (2004) 121.
[57] F. Padovani, R. Stratton, Solid State Electron. 9 (1966) 695.
[58] C. Crowel, V. Rideout, Solid State Electron. 12 (1969) 89.
[59] M.E. Aydin, O. Gullu, N. Yildirim, Physica B 403 (2008) 131.
[60] J. Osvald, Semicond. Sci. Technol. 18 (2003) L24.
[61] J. Osvald, Zs.J. Horvath, Appl. Surf. Sci. 234 (2004) 349.
[62] E. Dobrocka, J. Osvald, Appl. Phys. Lett. 65 (1994) 575.
[63] Zs.J. Horvath, Solid State Electron. 39 (1996) 176.
[64] Zs.J. Horvath, V. Rakovics, B. Szentpali, S. Puspoki, K. Zdansky, Vacuum 71 (2003) 113.
[65] S. Karatas, S. Altindal, A. Turut, A. Ozmen, Appl. Surf. Sci. 217 (2003) 250.
[66] J.H. Werner, H.H. Guttler, J. Appl. Phys. 69 (1991) 1522.
[67] A. Gumus, A. Turut, N. Yalcin, J. Appl. Phys. 91 (2002) 245.
[68] N. Marcano, A. Singh, F. Perez, Proceedings of the Second IEEE International Caracas Conference on Devices, Circuits and Systems, 1998 p. 88. doi:10.1109/ICCDCS.1998.705812.
[69] Lake Shore, Temperature Measurement and Control, Product Catalog and Reference Guide, vol. 1, 1995 pp. 1–10.